Investigations on the structural behaviour of archaeological heritage in Peru: From survey to seismic assessment

Rafael Aguilar [a,*], Rui Marques [a], Karim Sovero [a], Carol Martel [a], Fernando Trujillano [a], Ruben Boroschek [b]

[a] Department of Engineering, Civil Engineering Section, Pontificia Universidad Católica del Perú PUCP, Av. Universitaria 1801, San Miguel, Lima 32, Peru
[b] Department of Civil Engineering, University of Chile, Beauchef 850, Santiago de Chile, Chile

ABSTRACT

The conservation of archaeological heritage is of major importance for preserving the scientific, ethnographic and artistic values of past cultures. Once archaeological sites are exposed after being buried for centuries, they are subjected to natural hazards, which should be studied with up-to-date techniques. Moreover, conservation works are primarily focused on aesthetic aspects or on solving localized problems. In earthquake-prone areas, it is of extreme importance to carry out structural analysis studies for assessing the actual behaviour of archaeological constructions, and for proposing adequate intervention measures. This paper presents an extensive study on structural behaviour of archaeological building remains in Peru, based on in-situ non-destructive testing as well as on numerical approaches. The case of the Chokepukio Archaeological Site is presented, which was built between 1000 and 1450 AD in the Pre-Columbian era, with a mixed masonry of stone units and earthen mortar. The paper begins with a comprehensive description of the historical, architectural and structural aspects of the archaeological site. The possibility of applying operational modal analysis tests is then explored with reference to a representative wall of Chokepukio. The results of the experimental field campaign are used to develop calibrated finite element models of the wall, and to indirectly estimate mechanical characteristics of the masonry. Basing on the investigations performed, potential failure mechanisms are identified for the wall and validated by pushover analysis. Finally, the mechanisms are evaluated through kinematic limit analysis, to proceed with the seismic assessment.

© 2015 Elsevier Ltd. All rights reserved.

1. Introduction

Archaeological heritage buildings are like a constructed calendar of the history of civilizations, and thus are of high importance for the preservation of cultural, ethnographic and artistic values of past folks. Worldwide, archaeological remains represent a significant fraction of the heritage building stock. Much of these building remains, which are mostly made of masonry, have been discovered through archaeological excavations developed without consideration of structural aspects. Moreover, the exploration works introduce new hazards that can occur in open spaces, such as erosion due to water and wind, and particularly seismic events. Thus, the conservation of archaeological building remains requires, beyond a static stabilization or aesthetic operations, deep structural studies to assess its behaviour in case of exceptional loading events.

Peru has a great legacy of archaeological building remains, from typical earthen constructions in the coast to stone masonry remains in the Andean region. On the other hand, the Peruvian coast is located in the Pacific Ring of Fire, which makes this country a very relevant case regarding the development of a worldwide approach for the preservation of archaeological building remains. Recent seismic events such as the 2010 Chilean and 2003 Iranian earthquakes evidenced, once again, the high seismic vulnerability of historical constructions, in which archaeological building remains are included. Understanding the structural behaviour of this kind of constructions is particularly complex due to the difficulty for characterizing the geometry, materials and damage state, for identifying the structural system, as well as for creating reliable numerical models [1].

The International Council on Monuments and Sites (ICOMOS) has published different strategies for studying historical constructions. These strategies evidence the need for a deep knowledge of the monument under study, which can only be obtained through extensive experimental and diagnosis campaigns by means of laboratory and on-site investigations [2]. In this context, non-destructive testing is an important tool, since it allows the evaluation of constructions without endangering their structure.

---

* Corresponding author. Tel.: +51 1 6262000x4610; fax: +51 1 6262000x2813.
 E-mail address: raguilar@pucp.pe (R. Aguilar).

Vibration-based testing, namely Operational Modal Analysis (OMA), is a powerful non-destructive technique for the estimation of the structural dynamic properties of a construction. On the other hand, the structural evaluation requires adequate methods and tools for modelling and analysis, particularly regarding the seismic assessment. For this purpose, several approaches can be used concerning the nature and complexity of the construction, such as continuum finite element models, structural component methods or rigid block analysis, e.g. [3–7]. However, there are few studies applied to masonry remains and archaeological heritage, e.g. [8,9].

For this last kind of structures, the seismic assessment may require a multiple-view analysis approach, using different numerical methods for validating one against the others, and in which the Finite Element (FE) simulation is usually the reference for comparison, e.g. [8,10]. However, the development of a reliable FE model requires a calibration of the actual condition of the structure, regarding material parameters, boundary conditions and existing damage. This is usually made based on experimental in-situ vibration tests, trying to approximate the experimental modal properties by the numerical simulation, through a successive process of updating the model variables. In effect, calibration through vibration tests is an important issue in seismic analysis, e.g. [11].

This paper aims at the structural evaluation of archaeological heritage buildings, with application to the Chokepukio Archaeological Site in Cusco, Peru. The study includes on-site inspection, experimental testing, and numerical modelling and analysis, performed to assess the seismic vulnerability of the remaining traces of Chokepukio. After a brief description of the archaeological site, details of the OMA tests carried out on a representative wall of Chokepukio are given. Then, the optimization process of the FE model for the wall is presented, and finally, a pushover analysis is reported together with a kinematic limit analysis to proceed with the seismic assessment.

2. The Chokepukio Archaeological Site

The Chokepukio Archaeological Site is located 30 km from the city of Cusco, in the Andes of Peru. A wide variety of remaining structures made of stone masonry and mud mortar was found in the archaeological site. The seismic hazard at the region is high since the archaeological site is located in an area with active faults and Cusco itself is affected by the subduction of the Nazca plate.

Archaeological investigations in Chokepukio by McEwan et al. [12] evidenced that the original structures were built between 1000 and 1450 AD. Furthermore, artefacts were found in the site corresponding to Lucre and Killke cultures, which are considered ethnicities of transition between Wari (650–1000 AD) and Inca (1425–1532 AD) cultures.

Chokepukio presents a particular architecture of walls forming enclosures around open spaces (known as 'kanchas'). McEwan et al. [12] divided the site in three principal areas according to construction features and occupation periods, namely Sectors A, B and C (see Fig. 1a). Sector A, which is the one studied here, presents the highest density of standing structures (twelve 'kanchas' at least) and its walls enclose substantial areas (2600 m²) with small rooms connected amongst them. Sectors B and C correspond, respectively, to the beginning of the Inca occupation and post-Wari culture, and are more degraded. Isometric views of typical walls in each sector are presented in Fig. 1b–d.

The constructions at Chokepukio were built using andesite stone, which is an extrusive igneous rock named after the Andes. The masonry is composed of irregular stones interposed with mud-mortar joints of thickness ranging between 2.5 cm and 10 cm. The mortar is a mixture of local soil, clay, straw, and cactus resin. Unfortunately, there are no reported studies about material

mechanical parameters of the local andesite stone or masonry textures. Effectively, this gap needs to be addressed in future studies.

The height of the constructions ranges from 8 m to 10 m and each wall seems to be constructed in stages with growth in length and height, as evidenced by marked transitions amongst stone courses. Walls were built with multi-leaf arrangement and are 2 m width in average. In general, the walls present trapezoidal or rectangular niches at different heights. In some cases, the original earthen coatings are still visible on walls and niches.

One particular feature at Chokepukio is that higher walls have transversal buttresses, to improve vertical stability, and probably also to provide earthquake resistance. However, most of buttresses are partially in ruins, making the walls more vulnerable. In order to know the soil characteristics and foundation conditions, pit excavations were carried out near one wall located in the southeast corner of Sector A (see Fig. 2a and d). There it was possible to find the foundation of the wall, which is 3.0 m in depth and includes footings to increase the wall stability, see Fig. 2c and f.

3. Experimental diagnosis tests

In-situ experimental investigation was based on OMA [13], which was used as a vibration based non-destructive method to obtain the dynamic modal properties of the structure (frequencies, damping and modal shapes).

Rainieri and Fabbrocino [14] summarize the available techniques for OMA. These techniques consider the measured response of a structure under the unmeasured ambient excitations. Even if the input is not measured, it is assumed that the ambient excitation is banded with a bandwidth large enough to excite most of the response controlling modes. In general, the technique assumes a white noise ambient excitation to identify the modal response parameters. OMA is especially appropriate for civil engineering structures with high dimensions and special characteristics, where the application of impacts or shakers is too expensive or not feasible. Vibration based evaluation of existing constructions has become a deeply investigated topic, e.g. [15–18]. However, there are still few applications to archaeological heritage, e.g. [9,11].

OMA tests were carried out near the building remains located at the southeast corner of Sector A, namely on a couple of walls which present the particularity that are shored one against the other with timber struts (see Fig. 2a, b, d, and e). This sector was selected as case study due to the well preservation of the remaining structures, e.g. in the studied walls the original plaster is still on the interior face. For this study, only the front wall in Fig. 2 was instrumented, which presents variable geometry (thickness varies from 1.2 m to 1.8 m at the base and from 0.4 m to 0.6 m at the top), and average length and height of 20 m and 9 m, respectively. The wall presents two vertical parts with different stone masonry patterns. The bottom part is built with large stones and thin mud-mortar joints, while the top part is made of smaller stone units and thick mud-mortar joints. As shown in Fig. 2a–c, the change on masonry patterns coincides with the change on section in the height of the wall (at level +6.10 m).

For the experimental tests, sixteen measurement points were set in the wall in order to obtain an appropriate characterization of its dynamic response, see Fig. 3a. Due to the availability of a portable Data Acquisition System (DAQ) with a limited number of measurement channels, only four accelerometers were used for the tests. With this limitation, the test planning considered seven setups with two reference nodes (located at the expected higher modal amplitude points) and two roving sensors. The sensors layout was designed in such a way that the behaviour of the bottom and upper part of the wall could be properly measured. Sensors were criteriously installed in two rows at the bottom part of the
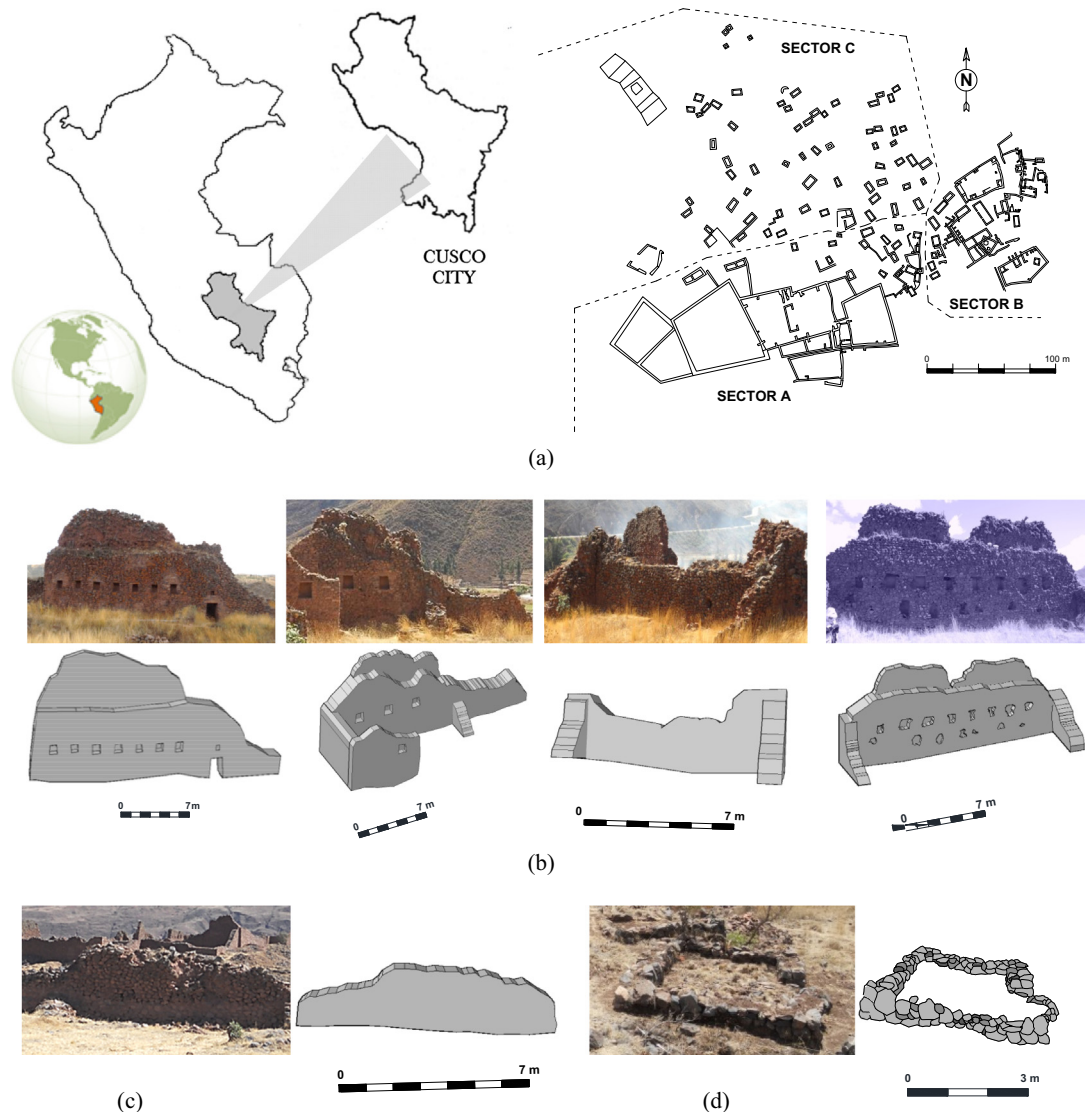
(a)

(b)

(c)

(d)

Fig. 1. The archaeological site of Chokepukio: (a) location in Cusco and plan of its sectors, and typical walls of (b) Sector A, (c) Sector B and (d) Sector C.

wall, namely at the level of niches and at the top (thickness transition section), which are considered as sections representative of the global behaviour. A third row of sensors was established at the mid-height of the upper part of the wall to capture the average behaviour of that zone.

In the case study here, highly sensitive sensors were used to capture the dynamic response in time domain. The root mean square values from the acceleration time series recorded in the tests (see Fig. 4) vary from 0.012 mg to 4.8 mg, while the noise level of the transducers is 0.001 mg rms. The transducers used were piezoelectric accelerometers with a sensitivity of 10 V/g and a dynamic range of ±0.5g together with a portable USB-powered 24 bits DAQ system (see Fig. 3b and c) with a maximum sampling rate of 51.2 kHz, bandwidth of 23.04 kHz, AC coupled (0.5 Hz), antialiasing filters, and 102 dB of dynamic range. As shown in Fig. 3d, an external scaffolding (not connected to the structure) was necessary to place the transducers along the wall. In this case, the accelerometers could not be fully fixed to the wall due to the intangibility of the monument, and thus, the transducers were screwed to metallic cubes that were conveniently perched in the wall. The sensors were placed on the wall in order to minimize any relative motion between the transducers and the wall. The

relative motion between the sensors and the wall was limited mainly by friction, and the rocking motions were avoided in the frequency of interest through an appropriated levelling of the sensors. Frequency analysis for each sensor indicated consistent and good quality records for frequencies below 10 Hz.

Regarding the acquisition time needed to obtain enough data for OMA purpose, Brincker et al. [19] propose a simple rule of thumb for the time length of recorded data, which is defined as inversely proportional to the product of the damping ratio by the natural frequency of a given mode. However, in this study and for all setups, the sampling rate was set to 200 Hz and the acquisition time to 10 min following the recommendation by Ramos [20] (sampling time in the order of 1000–2000 times the first natural period). To compute the averaged spectrum, the cross power density function was estimated using the Welch averaged modified periodogram method [21] and considering 1024 points as signal length, 50% as overlap criterion, and a decimation factor of 5.

The preliminary check of the signal quality was based on the analysis of the obtained averaged spectrum presented in Fig. 5a. The clear and well-spaced peaks shown in the spectrum evidence the high quality of the acquired signal. Based on this spectrum, a preliminary system identification was carried out using the Peak
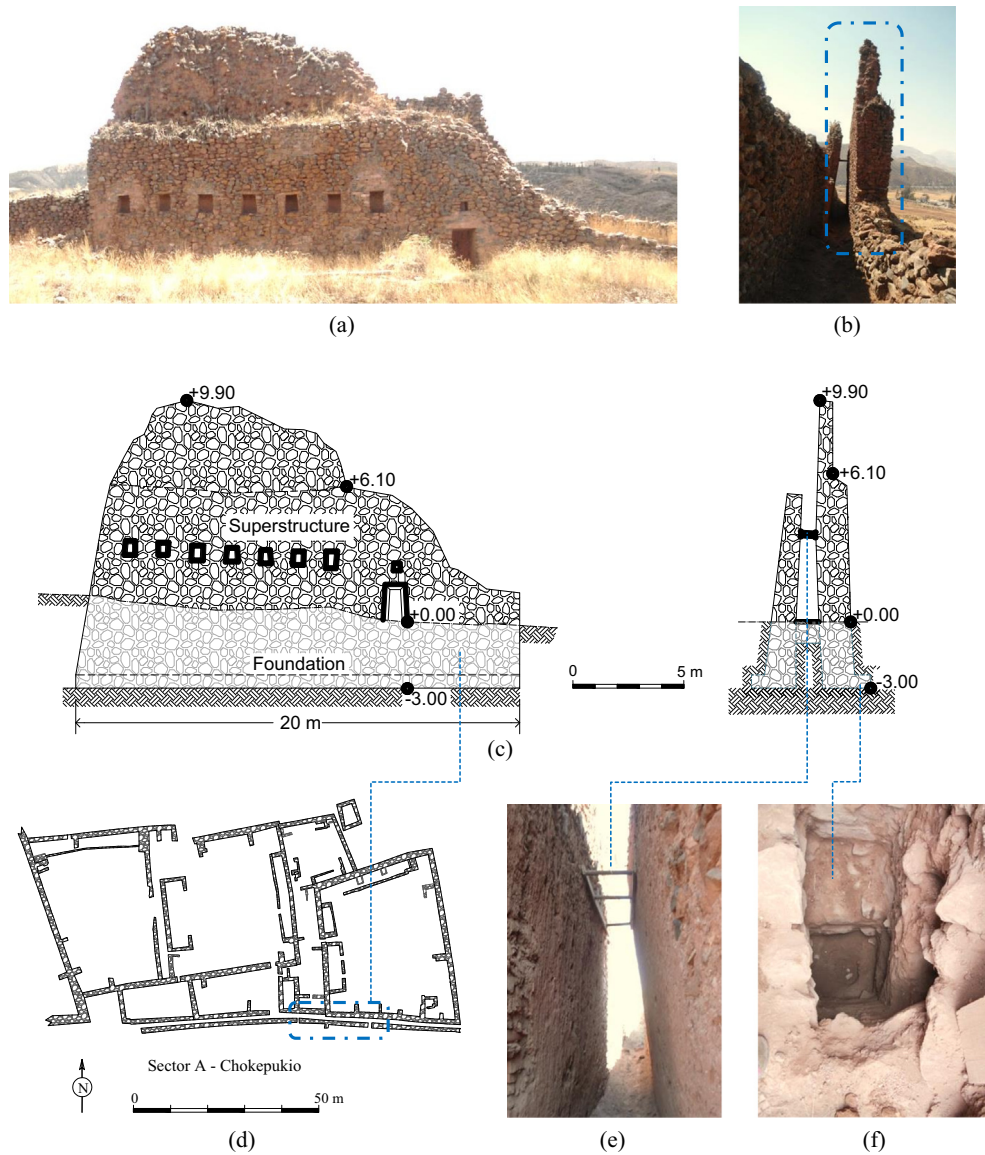
Fig. 2. General views of the studied area: (a) façade of the instrumented wall, (b) elevation of the instrumented wall, (c) front and transversal sections of the studied structure, (d) plan of the studied sector adapted from [12], (e) internal view of the two studied walls and (f) foundation detail.

Picking (PP) method [22,23]. The results of this processing denote a high flexibility of the wall, since at least the first seven natural frequencies are located below 10 Hz. These results were later confirmed using a more refined data processing technique, namely the Data-Driven Stochastic Subspace Identification (SSI-data) method [24] performed in ARTEMIS [25]. In this case, the perfectly aligned poles on the stabilization diagram in Fig. 5b confirm the accurate identification of the first seven modes. The results also show that the small or sharp peaks obtained in the averaged spectrum of Fig. 5a (peaks between the second and the third mode, the fourth and fifth ones, and the sixth and seventh modes) correspond to spurious modes, and should be discarded.

Table 1 reports a summary of the results of natural frequencies and damping ratios. As shown, frequency values present very low error margins (of less than 2%) comparing the results of the PP and SSI methods. Concerning the damping, it is know that the computed ratios from OMA tests are not precise, and furthermore the damping estimation is complex and very sensitive to the masonry type, but the predicted values around 3% are acceptable, e.g. [26].

The modal shapes identified with basis on the dynamic tests mainly denote out-of-plane deformations, as shown in Fig. 6a–g.

The first mode shape corresponds to a global translation motion of the wall with prevalence of displacements at its top part, where a slight oscillatory movement is observed. The second mode is through a global torsion of the wall and with the top part of the wall oscillating in its full length. The third mode shape is like a wing stroke of the top part of the wall that combines translational and rotational movements. The fourth mode denotes a global oscillatory motion of the wall, mainly around the vertical axis, and which presents large amplitude at the top part. The fifth, sixth and seventh modes are similar and correspond to local modes at the corners of the wall, where the displacements are concentrated through mixed motions.

In order to evaluate the quality of the estimations, the AutoMAC matrix is presented in Fig. 6h, which correlates the set of estimated mode shapes, in terms of the MAC ratio (see definition in Section 4.2), amongst themselves. The AutoMAC matrix confirms the quality of the dynamic identification of the first four modes,
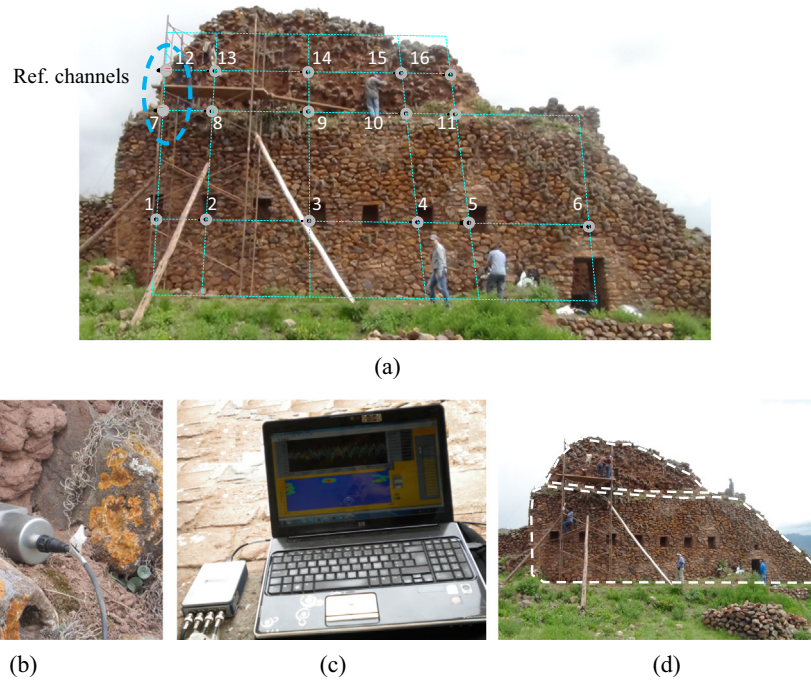
(a)

(b)   (c)   (d)

Fig. 3. OMA tests at Chokepukio: (a) test setup, (b) close up of a measurement node, (c) central acquisition station and (d) general view of the instrumented wall and the process of fixing sensors.

which are fully uncoupled, and denotes contamination between the measured degrees of freedom in the last three higher modes. This last aspect can also be due to the presence of a weak plane at the interface of the upper and bottom parts of the wall, and therefore the response is mainly characterized by lower modes. Thus, because of this predominant behaviour and of the location and limited number of sensors used in the tests, the higher modes were poorly captured. An aspect that could also have influenced the experimental results is the dynamic interaction between the instrumented wall and the other one located behind it, since the two walls share a common foundation and are somewhat connected through the timber struts that may behave in a nonlinear fashion. The study of this phenomenon might be of interest and should be considered in further experimental campaigns, particularly referring to the work of Rainieri et al. [27]. For further analysis stages, only the first four mode shapes were taken into account.

4. Numerical modelling

Today, advanced numerical tools are available with large application in the field of structural engineering, particularly Finite Element (FE) software. Here, a computationally sustainable approach for detailed modelling of complex structures is presented aiming at the development of an accurate model to support the seismic assessment of the studied wall in Chokepukio.

4.1. Model development

Three finite element models, which are presented in Fig. 7, were developed using DIANA [28] aiming at finding the numerical model that better represents the structure in study. Initially, the models were built considering the masonry as a homogeneous material with an elastic modulus of 800 MPa, according to reference values from Brignola et al. [29]. Considering that the density of the andesite stone in Cusco is about 2700 kg/m^3, and a slightly lower value

for the mortar density, the specific weight of the masonry is expected to be around 25–26 kN/m^3.

A first model (Model 1) which includes the instrumented wall and the other one located behind it, was built taking into account the interaction between the two walls through the three existing timber struts, as presented in Fig. 7a. The models were assembled using eight-node isoparametric brick elements of type HX24L. The timber struts are eucalyptus pieces with an elastic modulus of 15,000 MPa [30], which were modelled as beam elements of type L12BE. In Model 1, the timber struts were modelled as hinged to allow rotations around the vertical and orthogonal planes to the wall, and no possibility of sliding was considered. The boundary conditions of the timber struts were adjusted in order to approximate better the experimental modal properties. Even if the foundation of the structure and the restraining conditions below the ground may influence the mode shapes, particularly by the fact that the two parallel walls share a common infrastructure, it was considered that this effect is somewhat dissipated since the foundation is significantly deep and fully buried. Thus, for the sake of simplicity, the structure was assumed as fixed at the base. The walls were modelled with variable thickness in height corresponding to section changes. The thickness was also considered variable in the length of the instrumented wall, from 1.20 m on the left side, to 1.50 m from the door to the right side.

The second considered model (Model 2) was created assuming the instrumented wall as decoupled, and simulating the interaction from the timber struts through elastic springs with an equivalent axial stiffness, once the wooden struts are purely wedged between the walls (see Fig. 7b). Considering that the struts work in the range of small axial deformations with a low gradient compression-decompression behaviour, the adopted stiffness value is the complete axial component EA/L, where E is the elastic modulus of the wood, A is the cross-section area corresponding to a timber diameter of 0.1 m, and L is the strut length with a value of 1.0 m. The strut axial stiffness results with a value of 118.0 MN/m. Finally, a third model (Model 3) was built assuming the two walls
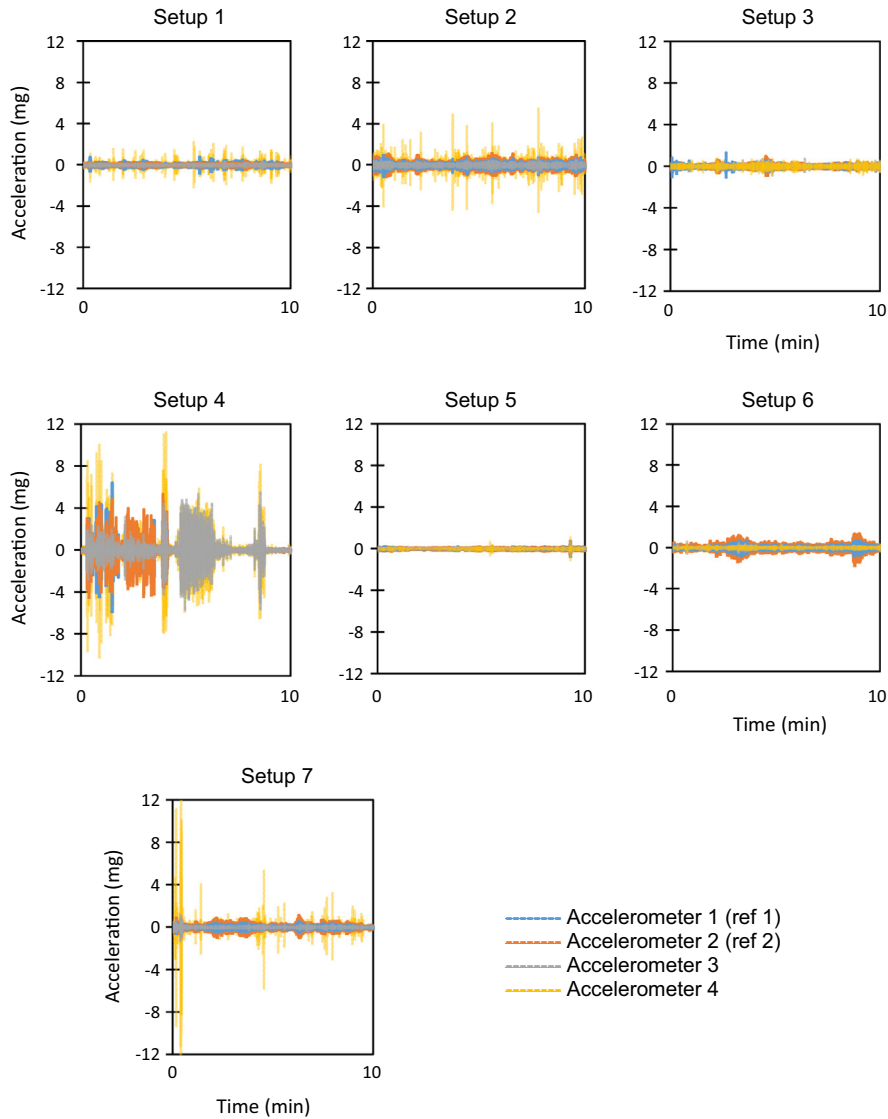
Fig. 4. Plots of acceleration time series obtained from the OMA tests.

as completely disengaged (only the instrumented wall is considered, see Fig. 7c).

As explained before, the numerical modal analysis and the subsequent model updating process were performed considering only the first four natural frequencies and corresponding modal shapes. In order to compare experimental and numerical modes, the Modal Assurance Criterion, MAC [31] and the Frequency scales with MAC combination, FMAC [32] were used. The MAC ratio is to provide a measure of consistency (degree of linearity) between estimates of a modal vector. In this case, it is computed through Eq. (1) to correlate the experimental and numerical modal vectors, respectively φ_{EXP} and φ_{FE}, and considering the set of n estimated degrees of freedom. In Eq. (1), the index FE corresponds to the results of the numerical simulation, while the index EXP refers to the experimental results. MAC values close to one indicate high correspondence, whereas values close to zero indicate poor resemblance. The FMAC is a graphical representation that provides a general comparison of experimental versus numerical modal properties from several mode shapes, by considering simultaneously the mode shape correlation (MAC ratio), the degree of spatial aliasing and the frequency comparison.

$$MAC = \frac{\left| \sum_{i=1}^{n} \varphi_{i,EXP} \varphi_{i,FE} \right|^2}{\sum_{i=1}^{n} \varphi_{i,EXP}^2 \sum_{i=1}^{n} \varphi_{i,FE}^2} \tag{1}$$

The results of frequencies, obtained for each model before the optimization process, are summarized in Table 2. Fig. 8 shows the FMAC graphs, where the MAC values and frequency scales are globally compared for the three numerical models. All models provide an accurate estimation of the first mode shape, with high MAC values (about 0.95) and a tolerable frequency difference (from 20% to 36%). However, Models 1 and 3 provide in general a better approximation concerning the second and third mode shapes, with MAC values from 0.86 to 0.92. These two models provide also better approximation between experimental and numerical frequencies, with a frequency difference from 20% to 37% when excluding the worst prediction by both models. The fourth mode was in general more difficult to capture with a good approximation in all models, i.e. MAC values lower than 0.57 and frequency differences from 31% to 49%. It can be noted that Models 1 and 2 seem to suffer some bias error [22], i.e. a deviation between the measured and predicted frequency while its range value increases.
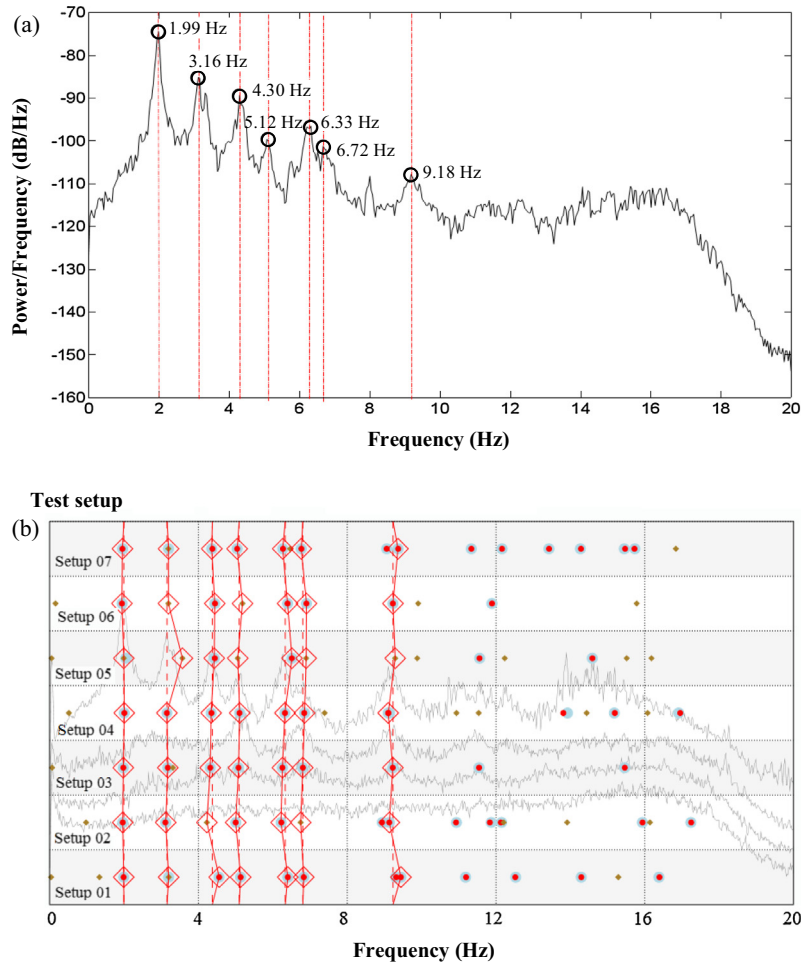
Fig. 5. Data processing results: (a) Welch spectrum for the PP method and (b) stabilization plot of the SSI method.

Table 1
System identification results from the experimental field campaign.

Mode	Peak Picking (PP)	Stochastic Subspace Identification (SSI)		Frequency relative error (%)
	Frequency (Hz)	Frequency (Hz)	Damping (%)	
1	1.99	1.98	2.6	0.51
2	3.16	3.19	3.2	0.94
3	4.30	4.39	3.2	2.05
4	5.12	5.08	2.2	0.79
5	6.33	6.29	2.4	0.64
6	6.72	6.70	2.6	0.30
7	9.18	9.19	3.0	0.11

Considering that the MAC ratio is a global indicator, the COMAC (Co-ordinate Modal Assurance Criterion) [20] was also evaluated, which allows to obtain local information from the measurement points. The COMAC ration is to identify which measurement degrees-of-freedom contribute negatively to a low value of MAC. In this case, it is computed through Eq. (2) for each degree of freedom (DOF) associated to a measuring point, and its value indicates the general approximation between the experimental and numerical modal displacements of the DOF, for the set of considered m mode shapes. The closer the COMAC value is to one, the more similar are the experimental and numerical modal displacements of a given DOF. The obtained COMAC values are presented in Fig. 9a, relating to the three considered models and according to the node numeration in Fig. 3a. Model 1 presents lower COMAC values for points located in the higher part of the wall, in particular the central node (in position 14), which can be because this wall part is significantly more flexible (presents larger displacements) than the remaining structure, and thus is more prone to errors. Models 2 and 3 present a similar approximation, but Model 3 is slightly better with reference to DOFs in the lower part of the wall.

$$COMAC_i = \frac{|\sum_{j=1}^{m} \varphi_{ij,EXP} \varphi_{ij,FE}|^2}{\sum_{j=1}^{m} \varphi_{ij,EXP}^2 \sum_{j=1}^{m} \varphi_{ij,FE}^2} \qquad (2)$$

All considered, Models 1 and 3 present similar approximations. However, due to the significant bias error at Model 1 and the simplicity of Model 3, this last one was selected for calibration through an optimization process.

4.2. Optimization procedure and results

The purpose of the optimization process is to find the most appropriate values for unknown variables (which are set at the beginning of the process) in order to approximate the numerical frequencies and mode shapes to those experimental. The process is monitored through computation of an error or objective function, which is minimized using a nonlinear least square method. The objective function is defined in Eq. (3), according to Ramos [20]. In this equation, the index FE corresponds to the results of the numerical simulation, while the index *EXP* refers to the experimental results.
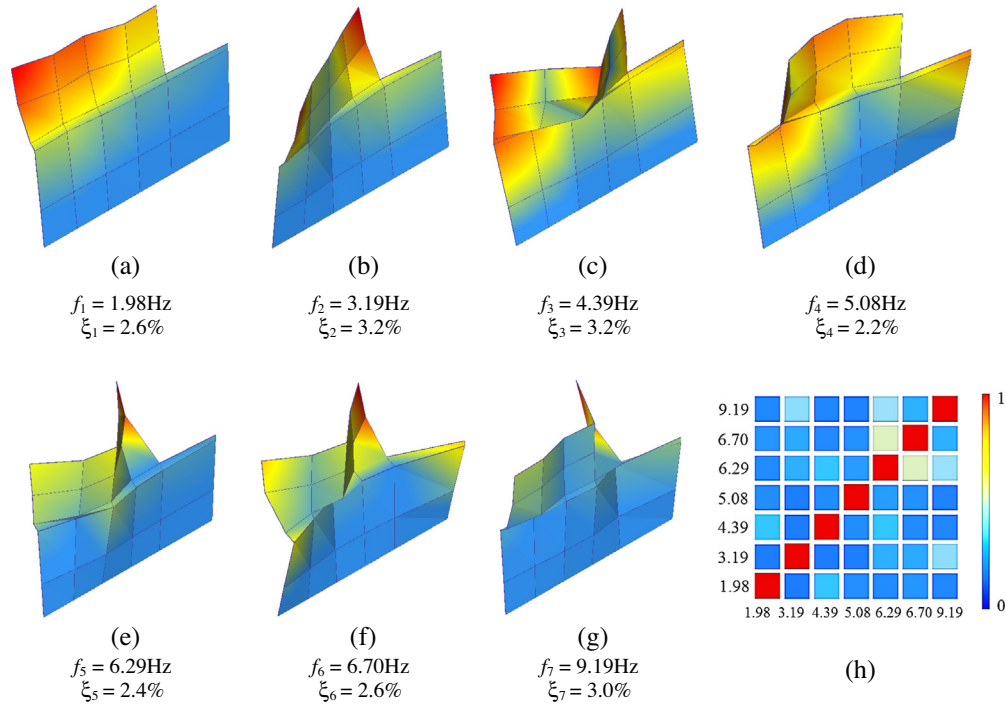
Fig. 6. Experimental mode shapes: (a–g) views of the first seven modes and (h) AutoMAC matrix.

(a) $f_1 = 1.98\,\text{Hz}$, $\xi_1 = 2.6\%$
(b) $f_2 = 3.19\,\text{Hz}$, $\xi_2 = 3.2\%$
(c) $f_3 = 4.39\,\text{Hz}$, $\xi_3 = 3.2\%$
(d) $f_4 = 5.08\,\text{Hz}$, $\xi_4 = 2.2\%$
(e) $f_5 = 6.29\,\text{Hz}$, $\xi_5 = 2.4\%$
(f) $f_6 = 6.70\,\text{Hz}$, $\xi_6 = 2.6\%$
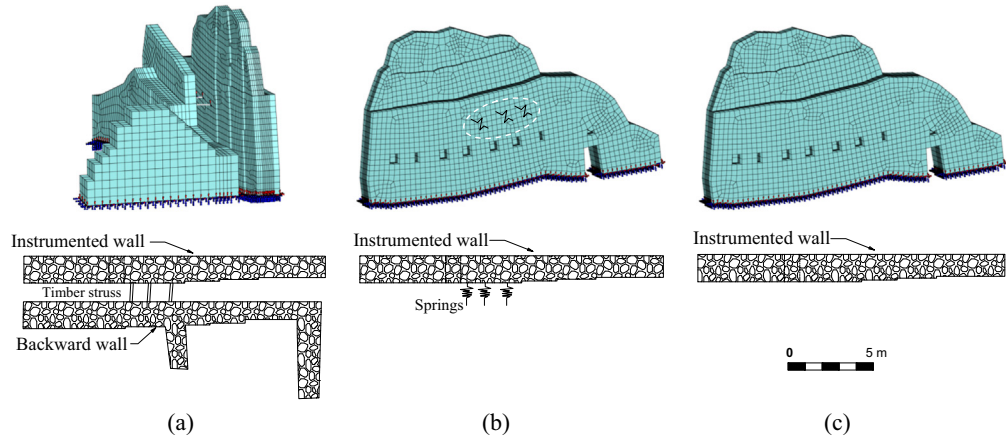(g) $f_7 = 9.19\,\text{Hz}$, $\xi_7 = 3.0\%$

Fig. 7. Developed FE models: (a) Model 1 considering interaction between walls, (b) Model 2 assuming the instrumented wall as decoupled and (c) Model 3 considering only the instrumented wall.

Table 2
Experimental and predicted frequency values obtained for each model.

Mode	Experimental (Hz)	Model 1 (Hz)	Model 2 (Hz)	Model 3 (Hz)
1	1.98	2.67 [34%]	2.72 [36%]	2.40 [20%]
2	3.19	4.81 [52%]	5.06 [60%]	4.32 [37%]
3	4.39	5.94 [36%]	6.36 [45%]	5.95 [36%]
4	5.08	6.67 [31%]	7.58 [49%]	7.41 [45%]

The difference in frequency is indicated inside brackets.

$$e = \frac{1}{2}\left[\sum_{j=1}^{m_w} W_{fj}\left(\frac{f_{j,\text{FE}}^2 - f_{j,\text{EXP}}^2}{f_{j,\text{EXP}}^2}\right)^2 + \sum_{j=1}^{m_\varphi} W_{\text{MAC},j}(\text{MAC}_{j,\text{FE}/\text{EXP}} - 1)^2\right] \quad (3)$$

where W refers to weighting matrices for frequencies (W_f) and MAC values (W_{MAC}), while m_w and m_φ are the number of considered natural frequencies and mode shapes, respectively. The frequencies and MAC parameters, $f_{j,\text{FE}}$ and $\text{MAC}_{j,\text{FE}/\text{EXP}}$, are made explicit according to Eqs. (4) and (5), which are based on the Douglas and Reid [33] approach. In these equations, V is the number of the unknown variables; X is the vector of the unknown variables; and A, B and C are constants which are computed through solving a system of equations considering base, lower and upper boundaries for the unknown variables ($2V + 1$ equations are considered). In the original formulation, the number of updating natural frequencies must be equal or larger than the number of unknown variables.

$$f_{j,\text{FE}} = C_j + \sum_{k=1}^{2V+1} A_{j,k} X_k + B_{j,k} X_k^2 \quad (4)$$

$$\text{MAC}_{j,\text{FE}/\text{EXP}} = C_j + \sum_{k=1}^{2V+1} A_{j,k} X_k + B_{j,k} X_k^2 \quad (5)$$
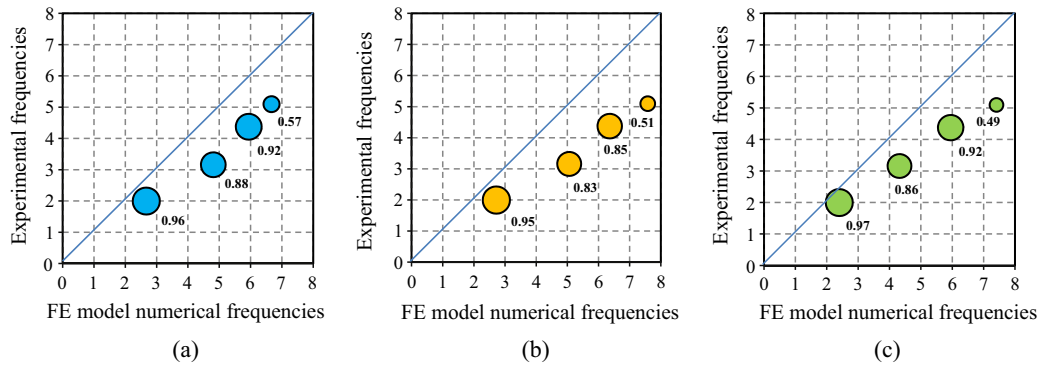
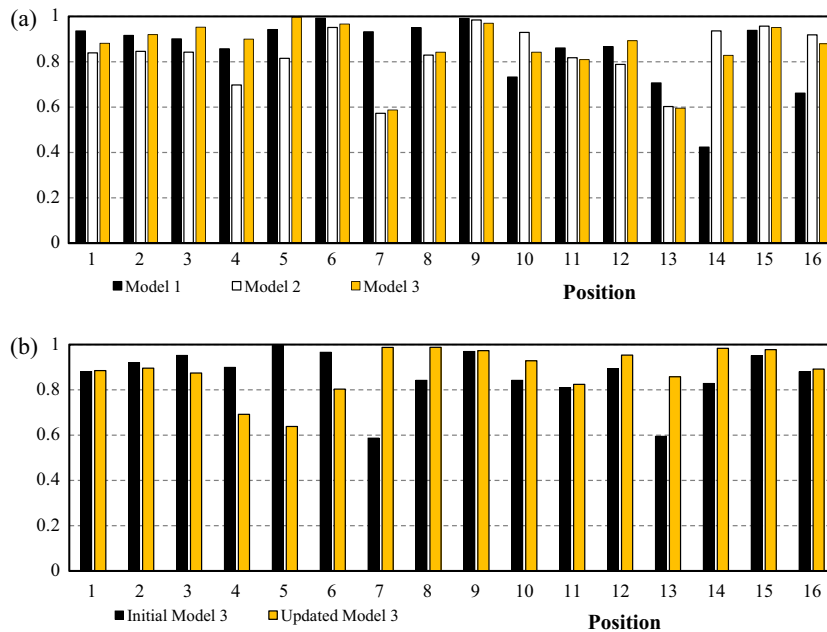**Fig. 8.** FMAC graphics for: (a) Model 1, (b) Model 2 and (c) Model 3 (frequency values in Hz).

Fig. 9. Comparison of COMAC values for all the measured DOFs, between: (a) initial Models 1–3 and (b) initial and updated Model 3.

In this study, the unknown variables were selected through sensitivity analysis, from an initial set that included geometrical aspects, boundary conditions and material properties. However, it is known that in general the numerical mode shapes present low sensitivity to global parameter variation, e.g. to the elastic modulus. Effectively, the conclusion was that the variables with more influence for changing frequencies were material properties (*E*-modulus and specific weight), while the modal shapes were mostly influenced by the geometry (different sections in length and height of the wall). There are studies in the literature specifically focused to FE model updating, namely using sophisticated formulations to perform model optimization at both global and local levels, e.g. [34,35]. In this work, local optimization has been only applied in a simplified manner, e.g. the geometry was locally changed based on personal sensitivity.

In effect, a first model was built considering the topographic survey and a preliminary manual modal shape tuning, but assuming only a thickness change between the bottom and top parts of the wall. Following, a third thickness change was additionally considered at the top part of the wall, see Fig. 7c, searching for a better approximation. This change of thickness is apparent in the real wall. Once the model geometry was set, a model calibration using the Douglas–Reid approach and an automatic optimization

process, were carried out considering the possibility of different masonry qualities for the bottom and top parts of the studied wall.

In this case, an interface exists between the two parts of the wall. However, from the on-site inspection it was not possible to conclude about the texture of the interface, but the transition between the two parts is probably made through interlocking of stone units in the two bodies. Under this hypothesis, a third zone in the wall is to be considered with an intermediate *E*-modulus value. However, due to uncertainty and for the sake of simplicity only two masonry qualities were considered with a perfect interface connection. In effect, the critical value for capturing the mode shapes is most likely the ratio of *E*-moduli rather than the individual values per se.

The application of the Douglas–Reid approach requires the definition of base, lower and upper bound values for the input variables (*E*-modulus and specific weight), which were set as presented in Table 3. While the base values are the assumed starting values for variables, the lower and upper bound values circumscribe the space of searching. The range of values in Table 3 was defined by identifying the bound values of the considered variables, for stone masonry. This range is not referred to a single optimization run, but to a sequence of runs for which the searching interval of parameters was successively changed in order to obtain

Table 3
Range of values for the updating variables.

	E-modulus (MPa)		Specific weight (kN/m³)	
	Bottom part (E_1)	Top part (E_2)	Bottom part (γ_1)	Top part (γ_2)
Base value	650.0	650.0	30.00	30.00
Lower value	300.0	210.0	20.00	20.00
Upper value	1300.0	1300.0	35.00	35.00

Table 4
Values for the updating variables obtained after optimization.

Updating variables	$E_{\text{bottom part}}$ (MPa)	$E_{\text{top part}}$ (MPa)	$\gamma_{\text{bottom part}}$ (kN/m³)	$\gamma_{\text{top part}}$ (kN/m³)
Initial value	650.0	650.0	30.00	30.00
Final value	579.7	210.1	25.32	25.27

a coherent (non-local) solution with a minimal error value. In some cases, the searching interval of parameters was purposely enlarged to extend the searching space, e.g. by considering an upper bound of 35 kN/m³ for the specific weight.

The optimization process was implemented by using the 'lsqnonlin' trust-region-reflective least squares algorithm available in Matlab [36], which is a search method based on minimizing the sum of the squares of the differences between the predicted and measured values. Fig. 10 shows the evolution of the objective function, and also of the values of the input variables against the number of iterations. As shown, the values became stable at the iteration 100, and convergence was attained after 300 iterations. Even if the objective function curve is practically flat after 150 iterations, the elastic modulus of the top part of the wall (E_2) follows with a slight variation (~9 MPa) until 300 iterations. It can be observed that E_2 is the last converged variable, and presents the larger value variation in the searching process.

The large decreasing of E_2 was in part due to large overestimation of its initial value. In effect, the masonry in the top part of the wall is most an earth-mortar/rubble stone mix, thus presenting a significant lower elastic modulus. Furthermore, the modal response is strongly determined by the deformability of the upper part of the wall. The results of the optimization process are summarized in Table 4. The final values for the varying parameters evidence a clear difference of the E-modulus for the masonry at the bottom and top parts of the wall, respectively with values of

580 MPa and 210 MPa. In the case of the specific weight, a value close to 25 kN/m³ is obtained for both parts.

The weighting matrices resulting from applying the Douglas–Reid approach are square diagonal matrices. In this case, the dimension of the weighting matrices is 9×9 as result of the combination of base, lower and upper values for a set of four mode shapes. In a first stage, these matrices were automatically calculated with the inverse of the normal variance of each modal quantity [20], and afterward, the matrices were adjusted to find a better solution for the optimization problem. The weight values are presented in the matrices in Eqs. (6) and (7), respectively for frequencies and MAC values, and which contain in each row a vector with the values of the main diagonal of the weighting matrices, in correspondence with the four considered mode shapes. Based on the obtained weights for MAC values, it can be noted the high sensitivity of the objective function to the first mode shape, while the fourth mode shape presents a small influence.

$$\begin{bmatrix} diag(W_{f,1}) \\ diag(W_{f,2}) \\ diag(W_{f,3}) \\ diag(W_{f,4}) \end{bmatrix} = \begin{bmatrix} 6.16 & 3.96 & 7.51 & 5.48 & 6.34 & 6.36 & 5.98 & 6.93 & 5.60 \\ 7.82 & 5.13 & 10.77 & 6.92 & 8.11 & 8.36 & 7.34 & 8.41 & 7.31 \\ 5.25 & 3.91 & 5.88 & 4.04 & 5.86 & 5.63 & 4.96 & 5.71 & 3.14 \\ 7.02 & 5.06 & 8.10 & 5.69 & 7.64 & 7.67 & 6.55 & 7.51 & 6.65 \end{bmatrix} \quad (6)$$

$$\begin{bmatrix} diag(W_{\text{MAC},1}) \\ diag(W_{\text{MAC},2}) \\ diag(W_{\text{MAC},3}) \\ diag(W_{\text{MAC},4}) \end{bmatrix} = \begin{bmatrix} 215.43 & 215.32 & 214.70 & 212.42 & 215.49 & 215.27 & 215.52 & 215.54 & 215.32 \\ 18.00 & 16.43 & 18.95 & 19.68 & 17.16 & 18.40 & 17.47 & 17.25 & 18.33 \\ 12.42 & 10.34 & 12.89 & 13.03 & 10.89 & 12.78 & 11.59 & 11.18 & 12.72 \\ 3.78 & 3.57 & 4.99 & 6.53 & 3.73 & 5.17 & 3.75 & 3.76 & 4.84 \end{bmatrix} \quad (7)$$
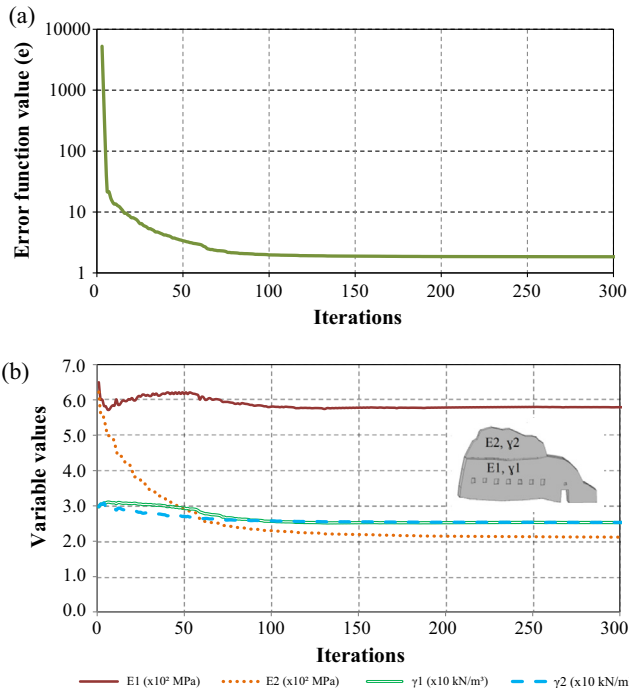
The reduced values of the elastic modulus for the studied wall are determined by the relatively low value of the E-modulus of the earthen mortar, since the local soils present a great deformability [37], and even if the mortar is improved with straw and cactus resin. On the other hand, Pinho et al. [38] report, for rubble stone masonry, an elastic modulus in the range 200–400 MPa and a compressive strength around 0.4 MPa, even if the compressive strength of the stone is about 50 MPa.

The FE model was then updated by considering the optimized values for variables. The final FMAC relationship, which is presented in Fig. 11a, denotes high correspondence between numerical and experimental frequencies and mode shapes: the maximum difference in frequencies is less than 8%, while the minimum MAC value is 0.86. For a better comparison, Fig. 11b and c presents the first four mode shapes regarding the experimental and numerical approaches. It is also to note the improvement, in general, of the COMAC values of the updated model relatively to those of the model before optimization, see Fig. 9b. Furthermore, it is observed in Fig. 9b that, for Model 3, while the COMAC values at the top part of the wall are improved after updating, the ones in the bottom part of the wall are worsened. In fact, this tendency of the COMAC values also reflects the accuracy of the numerical model.

Considering that the updated Model 3 is a better approximation to the reality, the lowest COMAC values are verified in the bottom-right part of the wall, where the points most distant to the
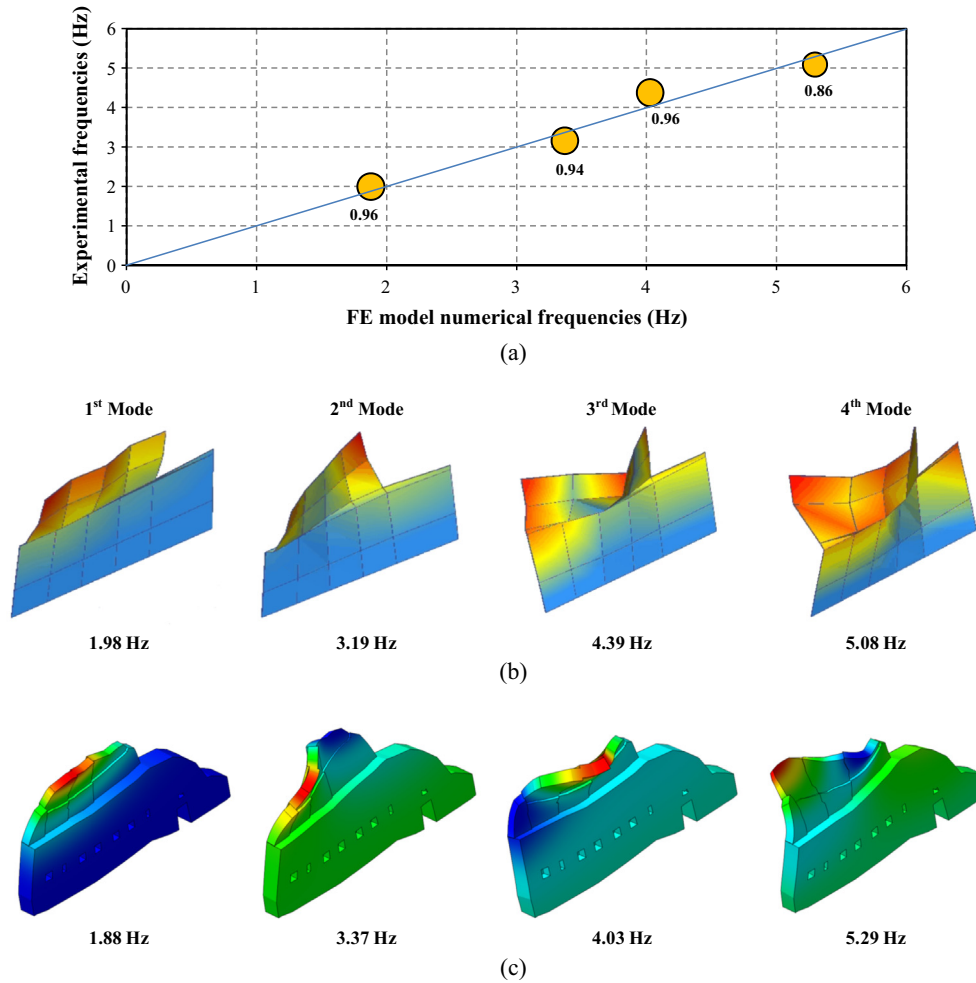

Fig. 10. Optimization process: (a) evolution of the objective function over iterations and (b) evolution of each variable over iterations.

Fig. 11. Experimental versus FEM mode shapes: (a) FMAC after optimization process, (b) experimental mode shapes and (c) FEM numerical mode shapes.

reference nodes are placed (in positions 4, 5 and 6). In effect, the COMAC values seem to suffer a kind of bias error, which increases with the distance to the reference nodes. The obtained results evidence the utility of the optimization process and the reliability of the updated model regarding its use in structural assessment.

5. Seismic assessment

The preoccupation with earthquake effects on buildings has been considered from ancient times, see [39,40]. The preservation of ancient constructions is also a great challenge for the future. Performance-based approaches have been proposed for the seismic safety assessment of structures, e.g. the displacement-based N2 method by Fajfar [41], which are however mostly applicable to the case of buildings with box behaviour [42]. The seismic assessment of structures without box action is generally more difficult to establish, since the walls present an almost independent behaviour and significant out-of-plane deformation and damage components. In this case, and particularly when dealing with complex geometries, the concept of structural performance needs most likely to be applied at local level, namely through reduction of accelerations and control of stresses. On the other hand, based on real and experimental evidence, it can be observed that walls tend to behave as rigid bodies subject to rocking, e.g. [43]. In the following, approaches for seismic assessment of wall structures based on

push-over loading and kinematic limit analysis are presented and applied to the case of Chokepukio.

5.1. Pushover analysis

Nonlinear static (pushover) analysis is an approach to evaluate the seismic response of buildings through simulating an incremental static lateral loading of the structure, as an alternative to nonlinear time-history analysis [42]. However, pushover analysis presents limitations, particularly the consideration of a negligible influence from the higher vibration modes, since the analysis fails in predicting local damages occurring previously to the considered mechanism. Certainly that a nonlinear dynamic analysis provides a more realistic seismic response, which is however highly sensitive to the seismic input and its uncertainties, and thus the pushover seems a more robust approach for practical purposes, see [44].

Once a nonlinear material law is considered, the pushover analysis allows capturing plastic and cracking events, and thus the inelastic source of the structure. Pushover has become a very popular approach for seismic design of real or idealized framed structures, for which the nonlinear behaviour is lumped in plastic hinges that are activated after a limit rotation is reached. For masonry structures, pushover has been mostly applied to planar models assembled through shell elements, which can normally include shear deformations through the wall length, but no bending, e.g. [8]. In cases of structures eminently three-dimensional and

strongly influenced by bending, modelling with brick solid elements is more adequate, since the formation of hinges is mainly due to flexural cracking.

However, it is known that the available material models in FE software are mostly validated with reference to bi-dimensional structures subjected to in-plane loading. Thus, further investigation is required to extend such models to a three-dimensional material domain, and to validate its accuracy in cases of out-of-plane mechanisms. Material models based on the Drucker–Prager criteria are commonly used for solid models of masonry constructions, which present advantages from the analytical and computational point of view, since the considered failure criterion presents a smooth failure surface, the masonry is considered as a continuum media and the model requires the definition of few parameters [45]. On the other hand, modelling the out-of-plane behaviour of masonry as a discontinuous material is difficult to handle in a FE context, and discrete element approaches have been developed with this purpose, e.g. [44].

For the Chokepukio case study, the nonlinear behaviour of the stone masonry was considered by the adoption of a constitutive law based on a total strain crack model, which considers an isotropic behaviour with a compressive cap and fixed smeared cracking [28]. This model is based on direct implementation of experimental observations, and furthermore, it provides stability in the cracking control and moderate computational cost [8]. Stress–strain relations were assumed considering exponential softening for tension and a parabolic law in compression. The post-cracked shear behaviour was considered assuming a shear retention factor of 0.1, to allow an important shear transference after crack occurrence. Based on the updated values of the E-modulus, the compressive strength was considered different for the two masonry patterns of the studied wall at Chokepukio, and its value is assumed as $E/500$, which is the mid-range relation of the interval proposed by Tomaževič [46]. The compressive fracture energy was defined by multiplying the compressive strength by a ductility factor equal to 1.6 mm [47]. The masonry tensile strength was assumed with a value of 0.1 MPa considering the relatively good

bond of the masonry, and the tensile fracture energy equal to 50 N/m [47]. The tensile strength adopted for the Chokepukio wall represents 10% of the assumed compressive strength for the masonry in the bottom part of the wall, which is a common assumption for masonry, e.g. [46]. This value was considered constant in the wall even though the bonding of the stones and mortar seems to be better in the upper part of the wall.

In this work, the pushover analysis was mainly performed to identify the critical sections and potential collapse mechanisms of the studied wall, and thus only the overturning of the wall to outside the principal façade was considered. The pushover was carried out under conditions of constant gravity load, and the lateral load pattern was assumed to be proportional to the mass regardless of the elevation. This load distribution was considered to allow a more direct comparison with the kinematic analysis, which considers mainly global rocking mechanisms. Given the large computational effort and non-convergence associated with the regular method when dealing with complex solid-based models, the modified Newton–Raphson method, combined with arc-length control and the line-search technique, was adopted to obtain the solution of the nonlinear problem.

Fig. 12 presents the evolution of the mechanism for the wall when subjected to the push-over loading proportional to the mass. The damage distribution was assumed as given by the vertical strains as an indication of cracking. As shown in Fig. 12a, after the elastic stage, cracking associated to bending tensile strains develops contemporaneously at the wall base and thickness transition sections, and a combined motion of the two parts of the wall is observed. These strains mainly generate sub-superficial cracks and produce a small degradation of the wall stiffness, which reflects in the capacity curve (segment a–b in Fig. 12e). The cracks spread in the wall face areas adjacent to the wall base and thickness transition sections (Fig. 12b). In the following stage, cracking concentrates in the wall base and propagates to inside the wall base, while the tensile strains in the top part are released. In this phase, the wall forms a plastic mechanism at the base, which is denoted in the plateau b–c of the capacity curve, and starts developing a
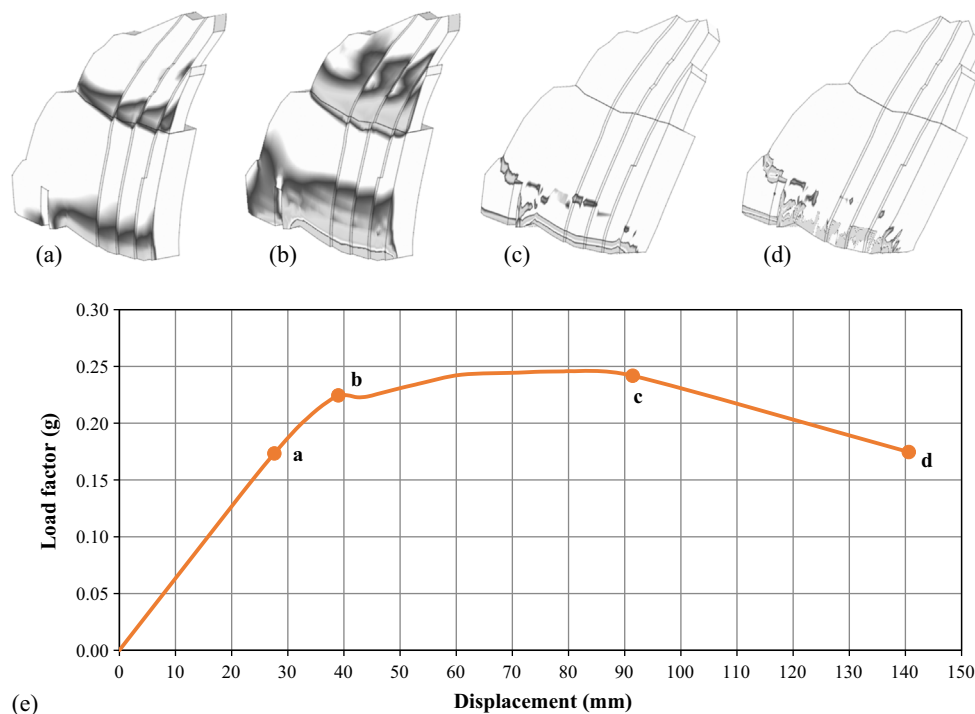

Fig. 12. Pushover analysis: (a–d) evolution of the wall mechanism with representation of vertical strains (as an indicator of cracking) and (e) capacity curve.

global rocking mechanism (Fig. 12c). Finally, the mechanism evolves with the damage propagating to within the wall base (Fig. 12d), and with the load factor decreasing in the capacity curve against increasing deformation (segment c–d in Fig. 12e). The identified sequence is fully evidenced in the capacity curve presented in Fig. 12e, which plots the load factor, defined as the ratio between the horizontal load and the wall weight, versus the displacement of a control point at the wall top.

The estimated push-over response according to the considered rocking mechanism will be used to validate the kinematic approach for seismic assessment presented in Section 5.2. However, it needs to be noted that the obtained results are in accordance with the typical behaviour verified for slender masonry elements failing by rocking, i.e. developing a hinge at the base and presenting a significantly ductile response.

5.2. Kinematic limit analysis

The plastic or limit analysis has been historically developed as a simplified approach for evaluation of structures that present a behaviour determined by the formation of plastic hinges and development of collapse mechanisms. In this case, a simplification can be assumed by considering a static equilibrium approach, such as that developed for the theory of arches [48]. For the case of masonry buildings, the common approach for limit analysis is based on macro-block discretization, by assuming collapse mechanisms for large structural assemblages. Even if limit analysis is very simple, it was included in seismic codes as a possible method for local failure assessment. The seismic verification of local mechanisms through limit analysis is specified in the Italian directive DPCM [49], which is addressed to heritage constructions. This regulation prescribes the application of the procedures specified in the Italian building code NTC [50] – Part 7: Design for seismic actions,

which are instructed for practical purposes in the CNTC [51] – Part C7: Design for seismic actions.

This procedure has been applied in seismic assessment of masonry structures complementarily to FEM-based approaches, e.g. [4,5,8]. Limit analysis is in general not sufficient for a full structural analysis under seismic loads, but it can be used to obtain a simple and quick estimation of collapse loads and failure mechanisms. This is probably the most realistic approach for practical seismic assessment of archaeological sites, which are generally constituted by a large set of substructures that are weakly connected and without forming a closed contour, e.g. Fig. 13.

The key of limit analysis is the definition of potential collapse mechanisms, which can be a relatively difficult task depending on the particularities of the structure. For a cantilever wall, a mechanism requires the formation of only one hinge, whose location is expected to be defined, under the lower bound theorem and corresponding to the inferior limit condition [48], with the thrust line touching the section edge, as illustrated in Fig. 14a. In this case, formation of hinges is also to be expected in sections with marked geometry change, as also confirmed in Section 5.1. After definition of the collapse mechanism, a kinematic approach is used to evaluate the load multiplier that activates the mechanism, α_0, which is the relationship between the horizontal load and self-weight applied to each body involved in the mechanism. Then, the solution for the equilibrium can be obtained through application of the principle of virtual work (PVW), which can be formulated (for a mechanism involving n bodies, m weight loads from dead bodies, and o external forces) according to:

$$\alpha_0 \left[\sum_{i=1}^{n} W_i \delta_{x,i} + \sum_{j=n+1}^{n+m} W_j \delta_{x,j} \right] - \sum_{i=1}^{n} W_i \delta_{y,i} - \sum_{h=1}^{o} F_h \delta_h = Int. Work \quad (8)$$

where W_k is the weight of the body k; $\delta_{x,k}$ and $\delta_{y,k}$ are virtual displacements of the body k relatively to its mass centroid, in x
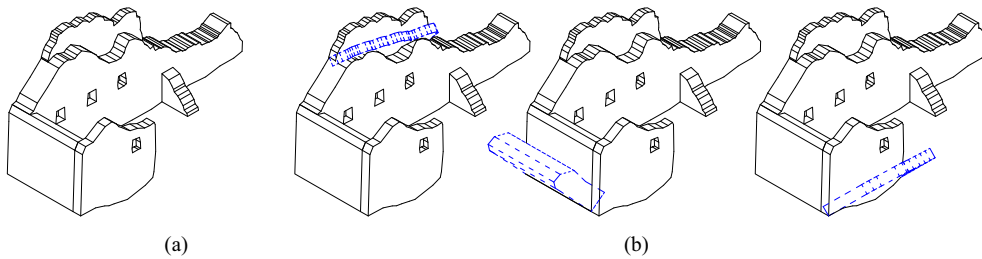

Fig. 13. Example of building remain: (a) view and (b) idealised potential collapse mechanisms.
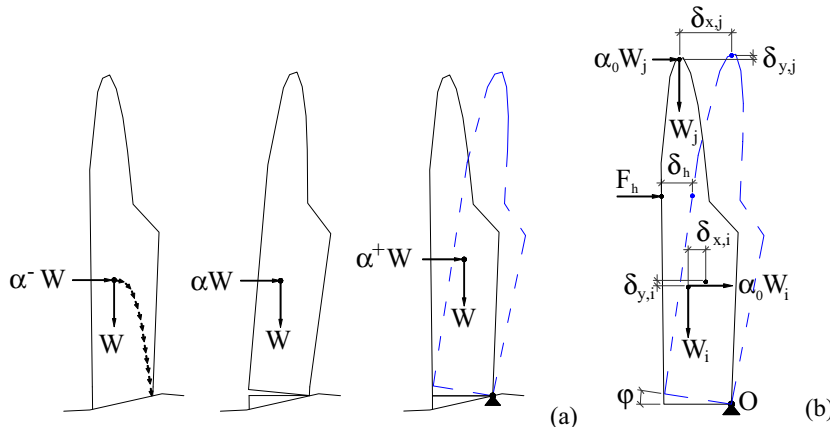

Fig. 14. Collapse mechanism for cantilever wall: (a) activation and (b) equilibrium variables.

(horizontal) and y (vertical) directions, respectively; F_h is an external force applied to a body and δ_h is its corresponding virtual displacement on the body; see Fig. 14b.

After activation of the mechanism, a progressive motion of the body occurs until reaching a maximum displacement state, corresponding to a zero value for the load multiplier (weight load vector is aligned with the hinge point), see Fig. 15a. The kinematic response considers the horizontal action that the structure is progressively able to stand with the evolution of the mechanism, until the complete dissipation of the horizontal force itself, i.e. as long as the structure is not able anymore of stand horizontal actions. The relationship between the load multiplier and the displacement d_k of a control point k can be assumed as linear according to Eq. (9) and Fig. 15b.

$$\alpha = \alpha_0[1 - d_k/d_{k,0}] \tag{9}$$

where $d_{k,0}$ is the displacement of the control point corresponding to a zero value for the load multiplier. This relation can be interpreted as a linear capacity curve, which is an approximation to the load–displacement response of the macro-block, and that is related with the assumptions of infinite compressive strength of the masonry and impossibility of sliding in the mechanism.

However, when assuming a limited compressive strength for the masonry, the difference between the actual relationship and the linear relationship is significant, because the actual relationship allows the displacement to increase comparatively quickly as the critical point (load factor becomes zero) is approached. In this case, the compressed edge at the wall base is crushed throughout the mechanism and the hinge moves to the interior of the edge section, which generates an asymptotic decreasing of the load factor against increasing displacement. However, this is not an issue for the case of thick stone masonry walls, since the compressive

strength is generally high and the crushed length of the edge section is relatively small comparatively to the wall thickness.

The appropriateness of applying the kinematic approach in the case of Chokepukio was evaluated through comparison of the mechanisms and capacity curves obtained from applying the pushover and kinematic analyses to the studied wall. Referring to the overturning of the wall to outside the principal façade, a rocking of the wall is identified from the pushover analysis similar to the global rigid-body mechanism assumed in the kinematic analysis. This is denoted in Fig. 16, where the kinematic curve present some features similar to those of the force–displacement pushover response that give sense to a comparison. It can be noted the matching of the two responses at the yield displacement of the pushover curve (40 mm), after that this curve slightly increases up to a displacement of 90 mm, and finally it decreases quicker than the kinematic curve due to internal damage to the wall. Furthermore, until the range of displacement verified for the pushover analysis (140 mm) the two curves denote energy equivalence, and they are matching for a decay of the maximum load factor in the pushover curve of 20% (to 0.2g), which is normally considered as the ultimate limit state for safety verification purposes through pushover methodologies.

5.3. Seismic safety verification in Chokepukio

In the following, aspects of the seismic assessment through kinematic limit analysis are presented considering the particularities of archaeological building remains in Peru. Finally, kinematic limit analysis is applied to the studied wall in the Sector A of Chokepukio.

For the seismic safety verification it is possible to proceed with an acceleration-based approach, which is the so-called linear kinematic analysis, or a displacement-based approach (nonlinear
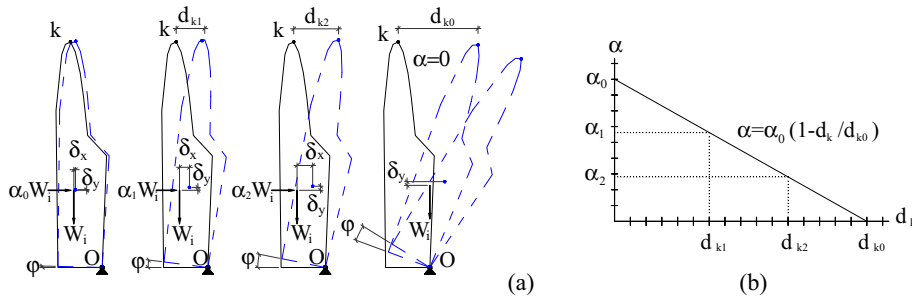

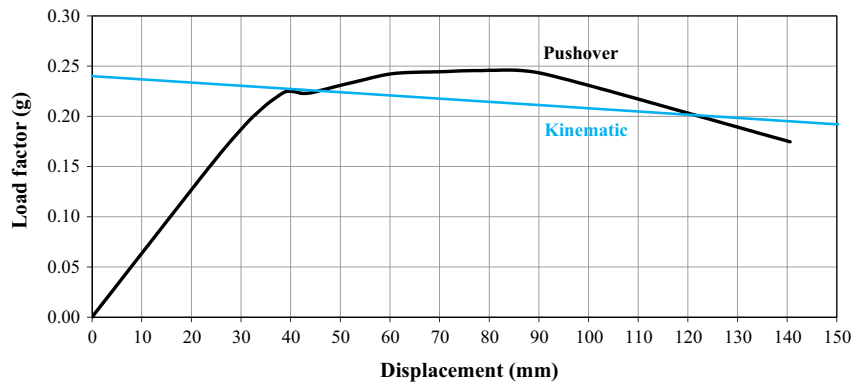**Fig. 15.** Evolution of mechanism: (a) motion sequence and (b) linear capacity curve.

Fig. 16. Comparison of capacity curves obtained from the pushover and kinematic analyses.

kinematic analysis), as specified in the Italian building code NTC [50] – Part 7. In the first case, the computed value of the collapse load multiplier, see Section 5.2, is used for a verification in terms of acceleration. On the other hand, the nonlinear kinematic analysis considers the load–displacement response to proceed with a safety verification in terms of displacement.

The capacity parameters need to be considered relatively to a single degree of freedom (SDOF) system, i.e. the capacity curve is to be transformed into a capacity spectrum through consideration of the dynamic properties of the structure, see Fajfar [41]. The formulation to obtain the capacity spectrum is not presented here in full, since it is detailed in the Italian building code NTC [50] – Part 7, from analogy with the capacity spectrum method by Fajfar [41]. For the particular case of a one-body mechanism, the spectral acceleration a^* can be computed as the product of the collapse load multiplier, α_0, by the gravity acceleration, g. Then, the spectral displacement d^* is computed according to Eq. (10), multiplying the real displacement of the control point k, d_k, by a modal participation factor. Thus, a linear relation is established for the capacity spectrum according to Eq. (11), where parameters a_0^* and d_0^* are respectively the collapse activation acceleration and the maximum spectral displacement in the capacity spectrum.

$$d^* = d_k \frac{\sum_{i=1}^{n+m} W_i \delta_{x,i}^2}{\delta_{x,k} \sum_{i=1}^{n+m} W_i \delta_{x,i}} \qquad (10)$$

$$a^* = a_0^*[1 - d^*/d_0^*] \qquad (11)$$

According to the Italian building code NTC [50] – Part 7, the seismic safety of buildings needs to be verified for both a damage limit state and a life safety limit state. In this work, only the life safety limit state, which considers a reserve of strength against collapse due to horizontal loads, is assumed as applicable to archaeological building remains. Note that the procedure for local seismic assessment as specified in the Italian building code has been mostly applied to existing structures, as referenced before. The safety verification in terms of acceleration is defined for two different cases of mechanism concerning the elevation level of the structure where the hinge is formed: at ground level which is denoted as 'global mechanism', and at an upper level of the structure which is denoted as 'local mechanism'. The two cases require, respectively, the verification of Expressions (12) and (13), where the right part is an equivalent formula to compute the spectral acceleration demand a_d^* according to the Peruvian seismic design code [52]:

$$a_0^* \geqslant \frac{a_g(P_{VR})S}{q} \equiv \frac{Z}{q} \cdot S \cdot g \qquad (12)$$

where in the Italian building code, $a_g(P_{VR})$ is the reference peak ground acceleration at the site, which is defined as a function of its probability of exceedance in a given reference period, P_{VR} (usually 50 years); S is the soil amplification factor; and q is the behaviour factor (assumed with a value of 2). In the Peruvian seismic design code, Z is the zoning coefficient; T_p is the period

corresponding to the end of the plateau in the elastic acceleration response spectrum; and T_1 is the fundamental vibration period of the structure.

$$a_0^* \geqslant \frac{S_e(T_1)\psi(z)\gamma}{q} \equiv \frac{Z}{q} \cdot \min\left(2.5\frac{T_p}{T_1}, 2.5\right) \cdot S \cdot g \cdot \psi(z) \cdot \gamma \qquad (13)$$

where in the Italian building code, $S_e(T_1)$ is the elastic spectral acceleration evaluated for the fundamental vibration period of the structure, T_1; $\psi(z)$ is the normalized first vibration mode of the structure, which can be approximated as the relationship between the elevation of the hinge and the total height of the structure, z/H; and γ is the modal participation factor, which can be approximated in function of the number of levels of the structure, N, as $3N/(2N+1)$.

Beyond the acceleration-based, the Italian building code NTC [50] – Part 7 also specifies a safety verification in terms of displacement. In this case, an ultimate spectral displacement d_u^* is defined correspondently to the life safety limit state as $0.4d_0^*$, mostly based on research by Doherty et al. [43]. Then, d_u^* is compared with the spectral displacement demand d_d^*, which is computed in function of a secant period T_s defined for the SDOF system as illustrated in Fig. 19a. Also here, cases of global and local mechanisms are considered, respectively requiring the verification of Expressions (14) and (15). In case of global mechanisms, d_d^* is obtained by intercepting the demand spectrum in correspondence with T_s.

$$d_u^* \geqslant S_{De}(T_s) = \frac{T_s^2}{4\pi^2} S_e(T_s) \qquad (14)$$

$$d_u^* \geqslant S_{De}(T_1)\psi(z)\gamma \frac{\left[\frac{T_s}{T_1}\right]^2}{\sqrt{\left[1 - \frac{T_s}{T_1}\right]^2 + 0.02\frac{T_s}{T_1}}} \qquad (15)$$

where $S_{De}(T_s)$ is the elastic spectral displacement evaluated for the secant period T_s, which can be related with the elastic spectral acceleration, $S_e(T_s)$, as presented in Expression (14).

Concerning the studied wall in Chokepukio, three collapse mechanisms have been considered as presented in Fig. 17, namely two global rocking motions around the wall base, and a partial rocking mechanism of the top part of the wall. The first global mechanism is purely through a rigid-body motion, while the second mechanism is constrained by the timber struts that are shoring the wall. The activation of this last mechanism requires the reaching of the axial load strength of the three wooden struts, which is considered as an external force applied to the wall. This force was evaluated by initially assuming a composite flexural behaviour of the timber rods. However, as the effective slenderness of each strut, i.e. the ratio between its effective length (0.9 m) and its diameter (0.1 m), is 9.0, according to the Peruvian wood design code [53] the strut is considered as a short column and thus behaves in pure compression. In this condition, the admissible compressive stress is taken as the compressive strength of the eucalypt wood, with a value of 7.8 MPa. Then, considering the full
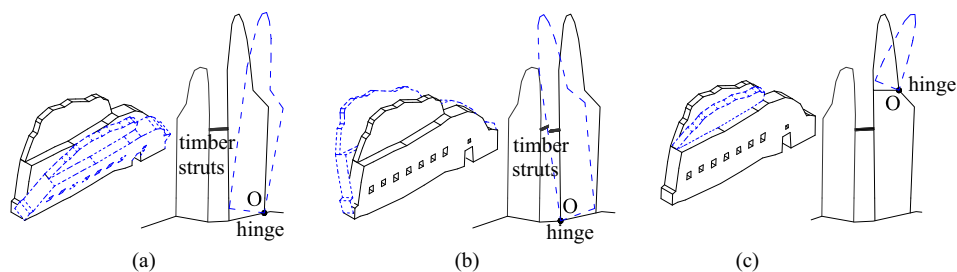

Fig. 17. Considered mechanisms: (a) 1st global rocking, (b) 2nd global rocking and (c) partial rocking.

diameter of the timber struts (cross-section area of 7855 mm^2), the total compressive axial strength has a value of 3×61.3 kN, i.e. around 184 kN. The third mechanism is through a rotation of the top part of the wall around a hinge located in the section with thickness change.

The limit analysis presents the advantage of requiring mostly a geometry input, beyond the specific weight of the material. In this case, a CAD-based tridimensional model of the wall corresponding to the calibrated geometry of the FE model was used for the computations, jointly with the optimized value of the masonry specific weight. The kinematics of the three considered mechanisms is illustrated in Fig. 18, from the initial static position to the free rotation stage. In this study, with only a body considered as involved in the kinematics, a virtual rotation is assumed around the edge hinge to apply the PVW as moment equilibrium (balance of the vertical and horizontal forces acting around the hinging point).

The seismic demand was considered according to the Peruvian seismic design code [52], which establishes a reference peak ground acceleration at the site (Zg) of 0.3g, corresponding to 10% probability of exceedance in 50 years (return period of 475 years). Considering the local ground, composed mainly of graved deposits, the soil factor S was considered with a value of 1.2 (medium soil in the Peruvian seismic design code). The period T_p, which is related to the soil type, was in this case computed from in-situ

microtremor (ambient vibration) measurements at the ground level. After applying the procedure by Nakamura [54] to estimate the ratio between the Fourier amplitude spectra of the horizontal (H) to vertical (V) components of ambient noise vibrations, i.e. the H/V spectrum, the predominant frequency was found in the range 2.0–2.5 Hz (0.4–0.5 s). Thus, an average value of 0.45 s was considered for the period T_p. The fundamental vibration period of the wall, T_1, was adopted as 0.53 s according to the modal analysis of the calibrated FE model.

The obtained capacity spectra for the three considered mechanisms are presented in Fig. 19b, where it can be observed that the second global rocking mechanism is the one that requires the highest value of spectral acceleration for its activation (0.27g). This is mainly due to the positive constraint effect by the timber struts, and even if in this case the 'pseudo-ductility' (displacement to acceleration ratio) results to be lower than that verified for the unconstrained global rocking mechanism. It can be noted that the timber struts, even if reacting with a small force, have a significant influence in the safety check. On the other hand, the partial rocking mechanism presents the lowest activation acceleration and is the most brittle. As shown in Table 5, the global rocking mechanisms are safe, both in terms of acceleration and displacement checks, while the partial rocking mechanism is unsafe and predictable to occur for a spectral acceleration of 0.17g.
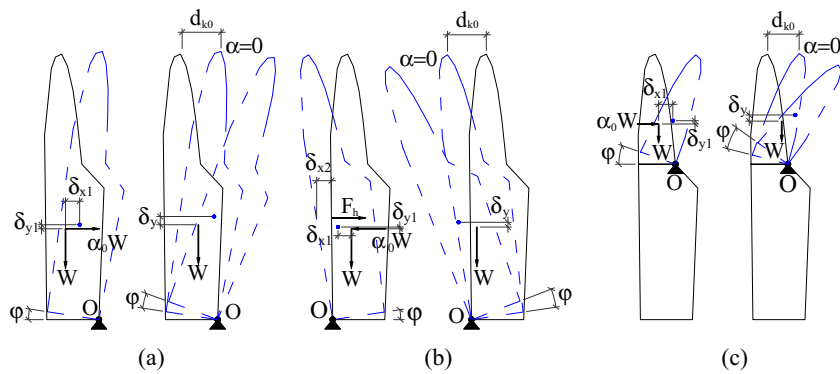

Fig. 18. Evolution of mechanisms: (a) 1st global rocking, (b) 2nd global rocking and (c) partial rocking.
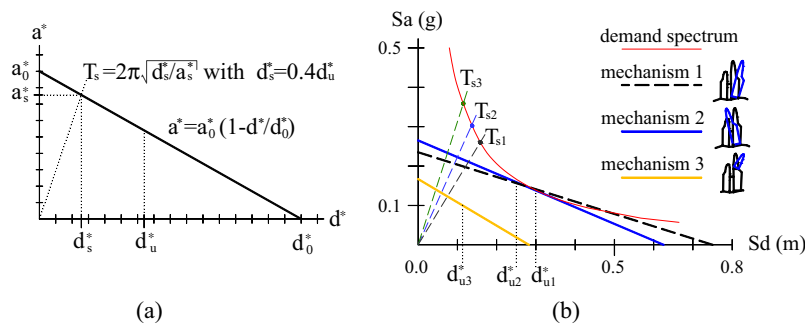

Fig. 19. Capacity spectrum: (a) definition and (b) computation for the considered collapse mechanisms.

Table 5
Results of limit analysis and seismic safety verification.

Mechanism	Capacity			T_s (s)	Demand		SF_a (g/g)	SF_d (mm/mm)	Check
	α_0	a_0^* (g)	d_u^* (mm)		a_d^* (g)	d_d^* (mm)			
1st global	0.24	0.24	300	1.53	0.18	155	1.33	1.93	Safe
2nd global	0.27	0.27	250	1.33	0.18	132	1.50	1.89	Safe
Partial	0.17	0.17	113	1.13	0.20	123	0.85	0.92	Unsafe

The partial mechanism results unsafe due to the considered amplification of the ground acceleration over the elevation of the wall, which implies a higher seismic demand. It is also noted as the check in terms of displacement provides in general higher safety factors comparatively to the force verification, which is mostly associated to the consideration of the dissipation of inertial horizontal force throughout the rocking motion, like a capacity reserve.

6. Conclusions

This paper presents investigations concerning the layout and structural behaviour of archaeological heritage in earthquake-prone areas, with an application to the Chokepukio Archaeological Site in Cusco, Peru. The study aims at providing general guidelines for structural evaluation of archaeological building remains, particularly regarding the seismic assessment. A multi-approach method was used that includes historical and typological surveys, and experimental, numerical and analytical investigations.

The survey of the site layout has large importance since it provides a general view of the problem and helps on selecting an adequate study strategy. In Chokepukio, a very particular layout was identified with contoured constructions forming an urban environment. Concerning the structural engineering point of view, it was possible to observe that the builders of Chokepukio used techniques to ensure the structural stability, namely the use of deep footings in foundations, and buttressing systems. On the other hand, the masonry pattern, the geometry and materials are complex and present large variability.

In-situ dynamic testing, namely OMA tests, was explored as a tool to support structural identification and assessment of archaeological heritage. For a proper test design of archaeological building remains, namely regarding the sensors layout, measurement chain and data processing techniques to use, it is important to consider the peculiarities of these sites, e.g. geometrics and boundary conditions. From the OMA tests performed at Chokepukio it was possible to accurately identify the relevant mode shapes for the studied sector, and the conclusion is that:

– the studied wall presents high flexibility, since at least the first seven natural frequencies are below 10 Hz. Furthermore, the first four frequencies of the wall are in the range 2–5 Hz, respectively varying from translational movements to oscillatory motions;
– the higher modes denote some contamination between measured degrees of freedom, which can be due to the presence of a weak plane at the interface of the upper and bottom parts of the wall, to limitations in the test setup or to effects of dynamic interaction with adjacent structures.

Numerical modelling was next developed which allowed, from a set of three Finite Element (FE) models initially considered, and based on measures of correlation between the experimental and numerical modal results, establishing an efficient model for further analytical purposes. This FE model was calibrated through sensitivity analysis and optimization routines, allowing the definition of optimal values for the elastic mechanical properties of the masonry (E-modulus and specific weight). The final obtained model presents high representativeness of the actual structural condition of the studied wall, concerning the approximation of the experimental modal response, i.e. maximum difference in modal frequencies is less than 8% while the lowest MAC value is 0.86. Furthermore, from the numerical modelling and calibration process of the FE model of the wall in Chokepukio, the following conclusions are pointed:

– the geometry, i.e. boundary conditions and section changes in height and length, plays a fundamental role when calibrating FE models, particularly to capture the modal shapes, and thus the need of tools capable of reproducing the geometric details is recognized;
– the most significant variables to capture the modal response in frequencies were the E-modulus, which ranges from 210 MPa to 580 MPa on the wall, and the specific weight (with a calibrated value close to 25 kN/m^3);
– the modal response is strongly determined by the deformability of the upper part of the wall, since the E-modulus of the this part of the wall varies largely during the optimization process. It can also be noted the high sensitivity of the objective function to the first mode shape of the wall.

Regarding the analytical investigation, a pushover analysis was carried out aiming at simulating an overturning mechanism of the studied wall. The obtained results allowed the design of simplified kinematic limit analysis taking into consideration the critical sections for the activation of collapse mechanisms. Kinematic analysis was then applied as a first approach for the seismic safety verification, after adapting the parameters of the Peruvian seismic design code in the safety conditions and considering different types of collapse mechanisms. Based on the analytical computations, it is concluded that:

– from the pushover analysis, the out-of-plane mechanism of the studied wall starts with flexural cracking at the wall base and thickness transition sections, after that, the cracks propagate in the thickness of the wall base and activate a rocking mechanism;
– the pushover and kinematic curves are matching at the yield displacement of the pushover response, the two curves denote energy equivalence, and they are coinciding for a decay of 20% of the maximum load factor in the pushover curve;
– from the kinematic analysis, the studied wall is safe regarding the global rocking mechanisms, which are activated for a spectral acceleration around 0.25g. However, the wall results unsafe respecting to a partial rocking mechanism of the top part of the wall, which is activated for a spectral acceleration of 0.17g.

The methodology applied in this study can be integrated in a broad tool for assessing the vulnerability of the entire archaeological site of Chokepukio and for studying other structures with similar characteristics. From this study, it was also possible to identify the need of further investigations aiming at experimentally characterizing the material mechanical parameters of the local masonry.

Acknowledgements

References

[1] Lourenço PB. Recommendations for restoration of ancient buildings and the survival of a masonry chimney. Constr Build Mater 2006;20(4):239–51.
[2] Roca P, Cervera M, Gariup G, Pelà L. Structural analysis of masonry historical constructions: classical and advanced approaches. Arch Comput Methods Eng 2010;17(3):299–325.

[3] Lourenço PB. Computations on historic masonry structures. Prog Struct Mat Eng 2002;4(3):301–19.

[4] Chellini G, Nardini L, Pucci B, Salvatore W, Tognaccini R. Evaluation of seismic vulnerability of Santa Maria del Mar in Barcelona by an integrated approach based on terrestrial laser scanner and finite element modelling. Int J Archit Heritage 2014;8(6):795–819.

[5] de Matteis G, Mazzolani FM. The Fossanova Church: seismic vulnerability assessment by numeric and physical testing. Int J Archit Heritage 2010;4(3):222–45.

[6] Ceroni F, Pecce M, Voto S, Manfredi G. Historical, architectural, and structural assessment of the bell tower of Santa Maria del Carmine. Int J Archit Heritage 2009;3(3):169–94.

[7] Casarin F, Modena C. Seismic assessment of complex historical buildings: application to Reggio Emilia Cathedral, Italy. Int J Archit Heritage 2008;2(3):304–27.

[8] Lourenço PB, Trujillo A, Mendes N, Ramos LF. Seismic performance of the St. George of the Latins church: lessons learned from studying masonry ruins. Eng Struct 2012;40:501–18.

[9] Chácara C, Zvietcovich F, Briceño C, Marques R, Peruccio R, Castañeda B et al. On-site investigation and numerical analysis for structural assessment of the archaeological complex of Huaca de la Luna. In: Proceedings of the SAHC2014: 9th international conference on structural analysis of historical constructions. Mexico City; 2014 [CD-ROM].

[10] Marques R, Pereira JM, Lourenço PB, Parker W, Uno M. Study of the seismic behavior of the "Old Municipal Chambers" building in Christchurch, New Zealand. J Earthquake Eng 2013;17(3):350–77.

[11] Oliveira DV, Grecchi G, McCall A, Noh J, Speer E, Tohidi M. Seismic analysis of the Roman Temple of Évora, Portugal. In: Proceedings of the 14th world conference on earthquake engineering. Beijing; 2008 [CD-ROM].

[12] McEwan G, Gibaja A, Chatfield M. Monumental architecture of late intermediate period of Cuzco: continuities of ritual reciprocity and statecraft between the middle and late horizons. Boletín de Arqueología PUCP 2005;9:257–80 [in Spanish].

[13] Magalhães F, Cunha A. Explaining operational modal analysis with data from an arch bridge. Mech Syst Signal Process 2011;25(5):1431–50.

[14] Rainieri C, Fabbrocino G. Operational modal analysis of civil engineering structures: an introduction and guide for applications. Berlin: Springer; 2014.

[15] Rainieri C, Fabbrocino G, Verderame GM. Non-destructive characterization and dynamic identification of a modern heritage building for serviceability seismic analyses. NDT&E Int 2013;60:17–31.

[16] Caprili S, Nardini L, Salvatore W. Evaluation of seismic vulnerability of a complex RC existing building by linear and nonlinear modeling approaches. Bull Earthq Eng 2012;10(3):913–54.

[17] Alaboz M, Ramos LF, Aguilar R. Dynamic identification and modal updating of S. Torcato church. In: Proceedings of the SAHC2010: 7th international conference on structural analysis of historical constructions. Shanghai; 2010. p. 110–16.

[18] Gentile C, Saisi A. Ambient vibration testing of historic masonry towers for structural identification and damage assessment. Constr Build Mater 2007;21(6):1311–21.

[19] Brincker R, Ventura C, Andersen P. Why output-only modal testing is a desirable tool for a wide range of practical applications. In: Proceedings of the international modal analysis conference IMAC XXI. Kissimmee; 2003 [CD-ROM].

[20] Ramos LF. Damage identification on masonry structures based on vibration signatures. PhD thesis. Guimarães: University of Minho; 2007.

[21] Welch PD. The use of the fast Fourier transform for the estimation of power spectra: a method based on time averaging over short modified periodograms. IEEE Trans Audio Electroacoust 1967;15(2):70–3.

[22] Ewins DJ. Modal testing: theory, practice, and application. 2nd ed. Baldock: Research Studies Press; 2000.

[23] Felber A. Development of a hybrid bridge evaluation system. PhD thesis. Vancouver: University of British Columbia; 1993.

[24] Peeters B, De Roeck G. Reference-based stochastic subspace identification for output-only modal analysis. Mech Syst Signal Process 1999;13(6):855–78.

[25] SVS. ARTeMIS structural vibration solutions extractor pro user manual, release 4.5. Aalborg: Structural Vibration Solutions; 2013.

[26] Elmenshawia A, Sorour M, Mufti A, Jaeger LG, Shrive N. Damping mechanisms and damping ratios in vibrating unreinforced stone masonry. Eng Struct 2010;32:3269–78.

[27] Rainieri C, Fabbrocino G, Manfredi G, Dolce M. Robust output-only modal identification and monitoring of buildings in the presence of dynamic interactions for rapid post-earthquake emergency management. Eng Struct 2012;34:436–46.

[28] TNO. DIANA: DIsplacement method ANAlyser, version 9.4.4. Delft: TNO DIANA BV; 2013.

[29] Brignola A, Frumento S, Lagomarsino S, Podesta E. Identification of shear parameters of masonry panels through the in-situ diagonal compression test. Int J Archit Heritage 2008;3(1):52–73.

[30] Sánchez-Acosta M. Characterization and use of E. grandis wood. In: Proceedings of the 'V Jornadas Forestales de Entre Ríos', Concordia; 1990. p. 83–93 [in Spanish].

[31] Allemang JR. The modal assurance criterion – twenty years of use and abuse. Sound Vib 2003;37(8):14–23.

[32] Ramos LF, Aguilar R, Lourenço PB, Moreira S. Dynamic structural health monitoring of Saint Torcato church. Mech Syst Signal Process 2013;35(1–2):1–15.

[33] Douglas BM, Reid WH. Dynamic tests and system identification of bridges. J Struct Div ASCE 1982;108(ST10):2295–312.

[34] Brownjohn JMW, Xia PQ, Hao H, Xia Y. Civil structure condition assessment by FE model updating: methodology and case studies. Finite Elem Anal Des 2001;37(10):761–75.

[35] Chellini G, De Roeck G, Nardini L, Salvatore W. Damage analysis of a steel–concrete composite frame by finite element model updating. J Constr Steel Res 2010;66(3):398–411.

[36] MathWorks. MatLab user manual, release 7.2. Natick MA: The MathWorks; 2011.

[37] García JM. Microzonification of the Cusco city. In: Proceedings of the '1er Simposium Nacional de Prevención y Mitigación de Desastres Naturales, Lima; 1987. p. 275–82 [in Spanish].

[38] Pinho FFS, Baião MFC, Lúcio VJG, Faria P. Experimental research on rubble stone masonry walls. In: Proceedings of the 1st historical mortars conference: characterization, diagnosis, conservation, repair and compatibility. Lisbon; 2008 [CD-ROM].

[39] Kirikov BA. History of earthquake-resistant construction: from antiquity to our times. Madrid: Instituto de Ciencias de la Construcción Eduardo Torroja; 1992.

[40] Stiros SC. Archaeological evidence of antiseismic constructions in antiquity. Ann Geophys 1995;38(5–6):725–36.

[41] Fajfar P. Capacity spectrum method based on inelastic demand spectra. Earthquake Eng Struct Dynam 1999;28(9):979–93.

[42] Lourenço PB, Mendes N, Marques R. Earthquake design and assessment of masonry structures: review and applications. In: Topping BHV, Costa Neves LF, Barros RC, editors. Trends in civil and structural engineering computing. Stirlingshire: Saxe-Coburg; 2009. p. 77–101.

[43] Doherty K, Griffith MC, Lam N, Wilson J. Displacement-based seismic analysis for out-of-plane bending of unreinforced masonry walls. Earthquake Eng Struct Dynam 2002;36(6):801–21.

[44] Casolo S, Uva G. Nonlinear analysis of out-of-plane masonry façades: full dynamic versus pushover methods by rigid body and spring model. Earthquake Eng Struct Dynam 2013;42:499–521.

[45] Pelà L, Aprile A, Benedetti A. Seismic assessment of masonry arch bridges. Eng Struct 2009;31:1777–88.

[46] Tomaževič M. Earthquake-resistant design of masonry buildings. London: Imperial College Press; 1999.

[47] Lourenço PB. Recent advances in masonry modelling: micromodelling and homogenisation. In: Galvanetto U, Ferri Aliabadi MH, editors. Multiscale modeling in solid mechanics: computational approaches. London: Imperial College Press; 2010. p. 251–94.

[48] Heyman J. The stone skeleton: structural engineering of masonry architecture. Cambridge: Cambridge University Press; 1997.

[49] DPCM. Directive for assessment and mitigation of seismic risk of cultural heritage, dated of 09-02-2011. Rome: Presidente del Consiglio dei Ministri; 2011 [in Italian].

[50] NTC. Norme tecniche per le costruzioni ('Italian building code'), Ministerial Decree dated of 14-01-2008. Rome: Ministero delle Infrastrutture e dei Trasporti; 2008 [in Italian].

[51] CNTC. Circular of instructions for application of the building code of 14-01-2008. Rome: Consiglio Superiore dei Lavori Pubblici; 2008 [in Italian].

[52] NTE.030. Reglamento de edificaciones del Perú, Norma técnica E.030: Diseño sismorresistente ('Peruvian seismic design code'). Lima: Ministerio de Vivienda, Construcción y Saneamiento; 2006 [in Spanish].

[53] NTE.010: Reglamento de edificaciones del Perú, Norma técnica E.010: Madera ('Peruvian wood design code'). Lima: Ministerio de Vivienda, Construcción y Saneamiento; 2006 [in Spanish].

[54] Nakamura Y. A method for dynamic characteristics estimation of subsurface using microtremor on the ground surface. Quart Report RTRI 1989;30(1):25–33.